Available online at www.sciencedirect.com
SCIENCE DIRECT®
Journal of Power Sources 150 (2005) 1–10
JOURNAL OF POWER SOURCES
www.elsevier.com/locate/jpowsour

Rotating ring-disc electrode measurements of manganese dissolution and capacity loss of $Li_{1+x}Mn_{2-x}O_4$ and $Li_{1+x}Al_yMn_{2-x-y}O_4$ spinel electrodes for lithium-ion batteries

Li-Fang Wang [a], Bor-Jian Fang [a], Jenn-Shing Chen [b,*]

[a] *School of Chemistry, Kaohsiung Medical University, Kaohsiung City 807, Taiwan, ROC*
[b] *Department of Applied Chemistry, National University of Kaohsiung, Kaohsiung City 811, Taiwan, ROC*

Received 17 November 2004; accepted 31 January 2005
Available online 16 March 2005

Abstract

Three types of spinel-based cathode powders, namely, $LiMn_2O_4$, $Li_{1.07}Mn_{1.93}O_4$, and $Li_{1.06}Al_{0.2}Mn_{1.74}O_4$, are examined with rotating ring-disc collection experiments to measure manganese dissolution and capacity losses in lithium-ion cells. The cyclic voltammograms are similar at high scan rates for all three electrodes. Initially, all electrodes rapidly lose capacity during cycling. After about 25 cycles, the electrodes start to exhibit capacity retention, and the performance matches that of the best spinels. The cation-substituted spinel electrodes experience a moderate capacity loss of 0.2% per cycle over 200 cycles, which is half that suffered by a typical spinel electrode ($LiMnO_4$). Manganese (Mn) dissolution from all the spinel-based samples is monitored in situ under various conditions. The ring cathodic currents for the cation-substituted spinel electrodes are similar to those for $LiMn_2O_4$, which shows that the Mn dissolution behaviour is the same for all spinel-based cathode powders. The ring currents reach maximum values at the end-of charge (EOC) and end-of discharge (EOD), with the largest peak at EOC. The results suggest that the dissolution of Mn from all spinel-based samples occurs during charge–discharge cycling, especially in a charged state at >4.0 V and in a discharged state at <3.1 V. In addition, lower ring cathodic currents are observed in the cation-substituted spinel cathodes and this indicates that the rate of dissolution of Mn has decreased in these materials.
© 2005 Elsevier B.V. All rights reserved.

Keywords: Lithium-ion cell; Spinel cathode ($LiMn_2O_4$); Cathode material; Rotating ring disc electrode; Manganese dissolution; Capacity loss

1. Introduction

In recent years, spinel $LiMn_2O_4$ has been studied extensively for lithium-ion (Li-ion) batteries as a cathode material because of its high voltage, low cost, and environmentally benign nature. These attractive characteristics make spinel $LiMn_2O_4$ a good candidate for use in large scale Li-ion batteries for electric vehicle (EV) and hybrid electric vehicle (HEV) applications [1]. Nevertheless, capacity fading during charge–discharge cycling is a problem for the spinel, particularly at elevated temperatures. It has been proposed that several factors contribute to capacity fading, namely: (i) electrochemical reaction with, the electrolyte at high voltage [2,3]; (ii) manganese dissolution into the electrolyte due to acid attack and a disproportionation reaction at the particle surface [4–7]: $2Mn^{3+}_{solid} \rightarrow Mn^{4+}_{solid} + Mn^{2+}_{solution}$; (iii) instability of the two-phase structure in the charged state leading to the loss of MnO and dissolution of Mn to a more stable single-phase structure [4,8,9]; (iv) formation of tetragonal $Li_2Mn_2O_4$ on the surface of spinel and the associated Jahn–Teller distortion at the end of discharge, especially under high current density, nonequilibrium conditions [5,10,11]; (v) formation of oxygen-deficient spinels [12]; (vi) cation mixing between the lithium and manganese sites in the spinel lattice [13]; (vii) loss of crystallinity during cycling [14,15].

Although many possible factors have been proposed that contribute to capacity fading of the spinel $LiMn_2O_4$ elec-

* Corresponding author. Tel.: +886 7 591 9463; fax: +886 7 591 9348.
E-mail address: jschen@nuk.edu.tw (J.-S. Chen).

0378-7753/$ – see front matter © 2005 Elsevier B.V. All rights reserved.
doi:10.1016/j.jpowsour.2005.01.043

trode, most of the evidence reported so far points to manganese dissolution at the top of charge as the major cause. Thus, it is essential to investigate the dissolution behaviour of the spinel electrode in order to reduce the level of capacity fading. In our earlier paper [16], Mn dissolution from a thin porous spinel $LiMn_2O_4$ electrode was measured using rotating ring-disc collection experiments. The in situ monitoring of Mn dissolution from the spinel $LiMn_2O_4$ electrode was examined in terms of cycle number, temperature, overcharge and overdischarge. The finding, provided a clear understanding of the Mn dissolution behaviour and the variation in manganese concentration in the electrolyte during cycling.

In order to minimize the solubility of the spinel electrode, several strategies have been followed over the years through substituting other cations for manganese in $LiMn_{2-x}M_xO_4$ (M: Li, Al, Ni, Mg or Cr) [17–19] or using an electrolyte with a salt other than $LiPF_6$ and eliminating water contamination [19,20]. The present study examines further the Mn dissolution behaviour of substituted manganese spinels using the rotating ring-disc electrode (RRDE) technique.

2. Experimental

Composite disc cathodes were prepared by wet coating, and were made from spinel-based cathode powders with acetylene black, SFG-6 (Timcal), and polyvinylidene fluoride (PVDF) binder (MKB-212C, Elf Atochem) in a weight ratio of 86:2:4:6. The spinel-based active materials, acetylene black and SFG-6 were first added to a solution of poly (vinylidene fluoride) (PVDF) in *n*-methyl-2-pyrrolidone (NMP, Riedel-deHaen). The mixture was stirred for 20 min at room temperature with a magnetic bar, and then with a turbine for 5 min at 2000 rpm to form a slurry that had the appropriate viscosity. The resulting slurry was coated on to a stainless-steel disc (diameter: 6 mm) and dried at 120 °C for 40 min. The resulting coating had a thickness of ∼100 μm and an active material mass of ∼2.4 mg. The quantity of active materials on the disc electrodes was kept constant (±0.2 mg) The electrodes were dried overnight at 100 °C under vacuum before being transferred to an argon-filled glove box for cell assembly.

The RRDE system (AFMT134DCPTT, Pine Instruments) with interchangeable discs consisted of the above electrode and a Pt ring electrode (width: 1 mm) that were separated with a 0.5 mm gap. The collection efficiency when using this geometry was 0.24. The rotating ring-disk assembly was operated by means of a Pine AFMSRX rotator and a CH705 Bipotentiostat (CH Instruments) with a computerized interface. The manganese dissolved from the disc electrode was collected at the Pt ring. Lithium foil (Aldrich) was used for both the reference and the counter electrodes. A schematic of a glass-beaker cell containing the RRDE system was given in our earlier paper [16]. A solution of $LiPF_6$ (1.0 M) in a 1:1 (v/v) mixture of ethylene carbonate (EC) and dimethyl carbonate (DMC) was used as the electrolyte (Ferro Corp.).

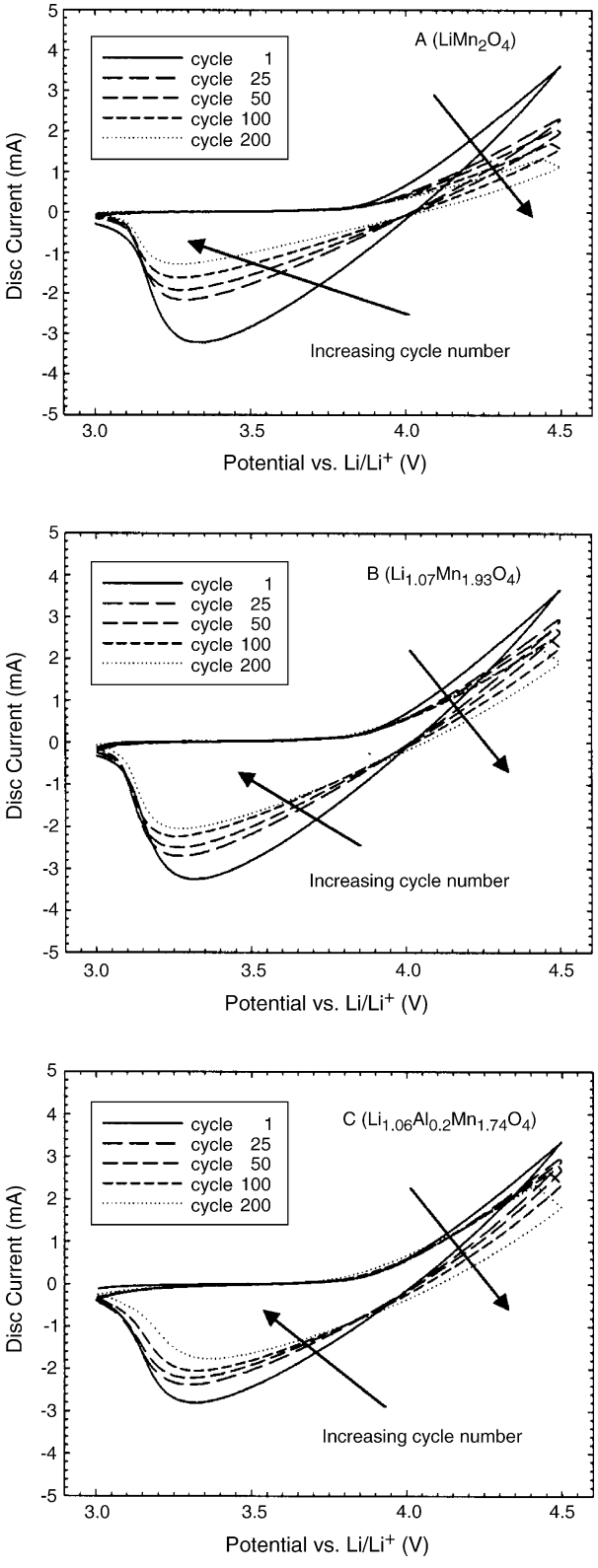

Fig. 1. Cyclic voltammograms for representative groups of spinel-based electrodes cycled between 3.0 and 4.5 V at 10 mV s^{-1} and 500 rpm with 1 M $LiPF_6$ + EC/DMC (1:1) at 1, 50, 100, 150 and 200 cycles at 30 °C.

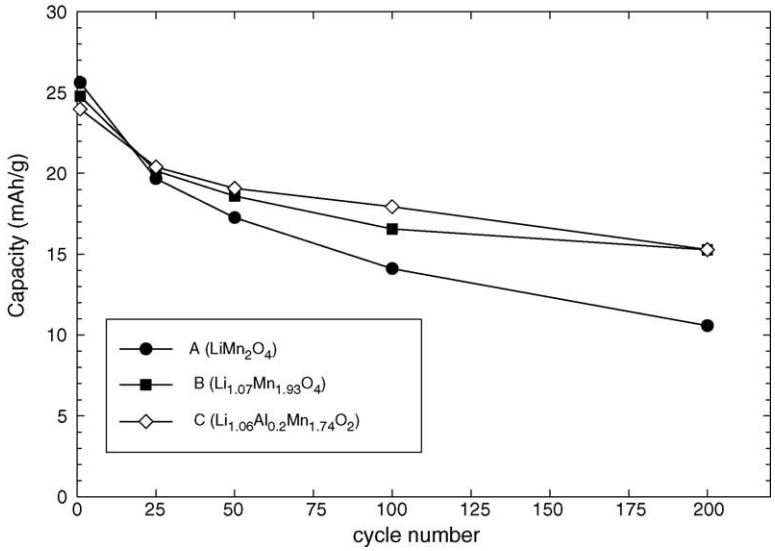

Fig. 2. Variation of discharge capacity as function of cycle number for representative groups of spinel-based electrodes cycled between 3.0 and 4.5 V at 10 mV s^{-1} and 500 rpm with 1 M $LiPF_6$ + EC/DMC (1:1) at 1, 50, 100, 150 and 200 cycles at 30 °C. Capacity calculated from cyclic voltammograms.

During cyclic voltammograms, the potential of the spinel-based disc electrode potential was scanned between 3.0 and 4.5 V versus Li/Li^+ at 10 mV s^{-1}. The Li anode was isolated from the cathode by two layers of Celgard 3401 separator, and the Li reference electrode by a vycor tip to avoid dissolved Mn ions being deposited on the Li anode and reference electrode. For the in situ cell test, the spinel-based disc was cycled at 100 mV s^{-1} between 3.0 and 4.5 V or an extended voltage range at various conditions while the ring was held at 1.0 V to collect the Mn^{2+} ions generated from the disc electrode. Three tests were carried out for each condition and the average performance was recorded. The cell fabrication and all measurements were carried out in a glove-box filled with dry argon.

3. Results and discussion

The performance of three groups, A, B, and C, which represent the spinel-based cathode powders $LiMn_2O_4$, $Li_{1.07}Mn_{1.93}O_4$, and $Li_{1.06}Al_{0.2}Mn_{1.74}O_4$, respectively, was investigated. Cyclic voltammograms (CVs) were obtained at room temperature (∼30 °C) between 4.5 and 3.0 V versus Li/Li^+ at 10 mV s^{-1} and 500 rpm. The resulting data for samples A, B, and C at 1, 50, 100, 150, and 200 cycles,are shown in Fig. 1. The shapes of these curves are similar at a very high scan rate (10 mV s^{-1}), although the height of the peak decreases during consecutive cycling. In general, the CV of the spinel electrode exhibits two peaks located at 4.03 and 4.17 V on charge and at 3.99 and 4.10 V on discharge. The peaks correspond to the two-step reversible (de) intercalation of lithium between $LiMn_2O_4$ and λ-MnO. At a high scan rate, however, the reaction zone is limited to a small thickness on the surface of the electrode and the two peaks are not well separated. The disc current is only observed after 4 V on the anodic scan (during charge) and decreases continuously until 3.3 V on the cathodic scan (during discharge). Both the anodic and cathodic peak currents for all samples decrease significantly during the first 25 cycles, especially for sample A. This suggests that the spinel-based disc electrodes, which initially rapidly lose capacity with cycling, begin to exhibit capacity retention after 25 cycles cycling. This behaviour matches that of the best spinels. A plot of high-rate discharge capacity versus cycle number for all samples is shown in Fig. 2. The discharge capacity is calculated from the CVs in Fig. 1. The discharge capacity declined to less than 10 mAh g^{-1} for sample A and to 15 mAh g^{-1} for samples B and C by the end of 200 high-rate cycles. As has been commonly reported in the literature, the cation-substituted samples (B and C) clearly show much better cycling performance than typical spinel, $LiMn_2O_4$ (A) [5,15,18,22–26]. Among these samples, sample C shows the best retention of capacity in spite of its slightly lower initial capacity. Substitution of Mn by cations reduces the capacity of the spinel for

Table 1
Rate of capacity loss for representative groups of spinel-based electrodes cycled between 3.0 and 4.5 V at 10 mV s^{-1} and 500 rpm with 1 M $LiPF_6$ + EC/DMC (1:1) at 30 °C.

Sample group	Cycle number	Initial capacity (mAh g^{-1})	Capacity loss per cycle (%)	Capacity loss after 200 cycles (%)
A ($LiMn_2O_4$)	200	25.6041	0.4412	58.7
B ($Li_{1.07}Mn_{1.93}O_4$)	200	24.7672	0.2414	38.33
C ($Li_{1.06}Al_{0.2}Mn_{1.74}O_4$)	200	23.9733	0.2246	36.22

lithium in the 4-V region since these ions are not oxidized or reduced over this potential range [26]. In our previous paper [16], we demonstrated that the rapid initial capacity fading of the spinel electrodes is not caused by the simple dissolution of Mn, because the Mn dissolution rate is almost constant prior to 150 cycles. Other possibilities for capacity fading are structural change and electrolyte decomposition [8]. Amatucci et al. [27] proposed that spinel electrodes with small spinel lattic parameters or higher manganese average oxidation states exhibit good capacity retention during cycling. The performance of samples B and C with cation-substituted spinel cycles is significantly better due to their higher average oxidation state and smaller lattic parameter. The smaller ionic radii of Li^{+} and Al^{+3} ions that replace the Mn^{+3} with larger ionic radii at their crystal sites causes the shrinkage of the lattice in samples B and C. In addition, Yoshio et al. [24] reported that replacing the Mn^{+3} ion by Al^{+3} increases the average oxidation state of the Mn ion, and helps to retain an average Mn valence higher than 3.5 in the $LiAl_xMn_{2-x}O_4$ powder. It also works to maintain a single phase throughout the charge–discharge process. Calculations of the rate of loss of capacity and the capacity per cycle are listed in Table 1; both are based on the electrode performance on the continuous cycles at a high scan rate shown in Fig. 1. The capacity loss rate, expressed as percentage per cycle, is based on the initial discharge capacity [21]. The capacities of all the sam-

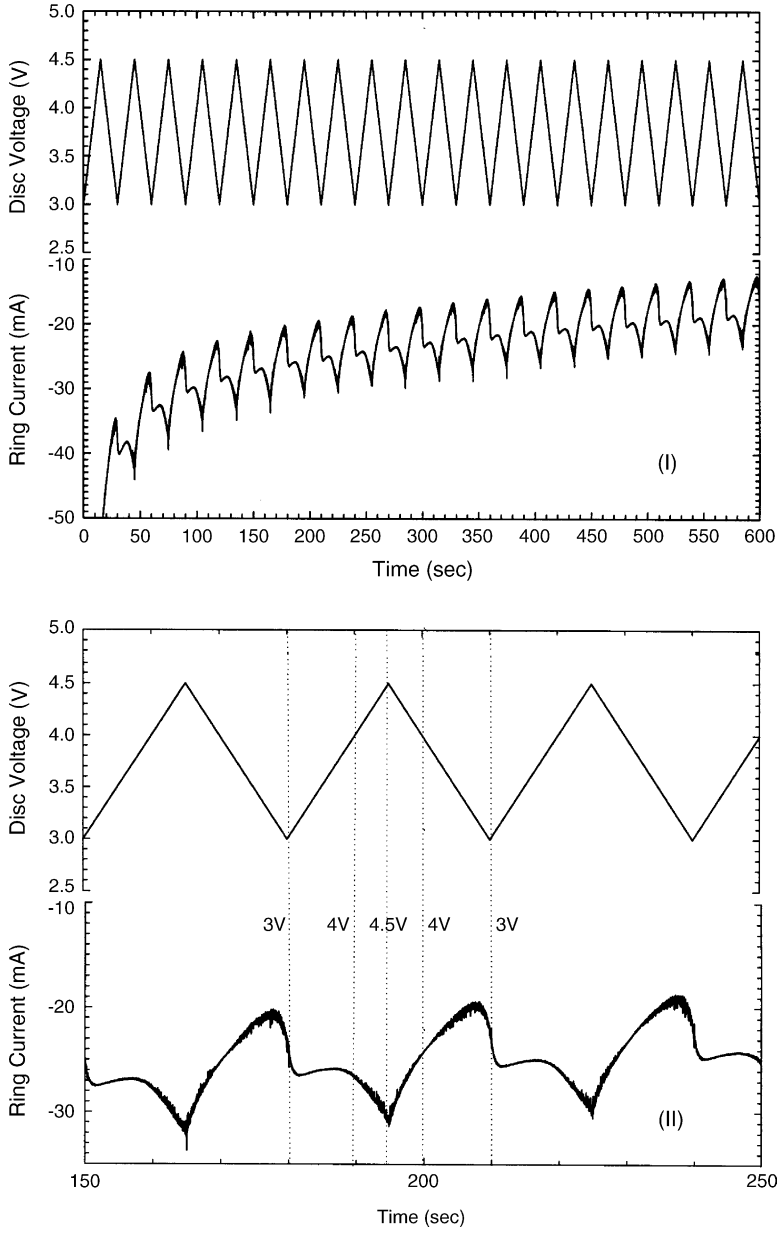

Fig. 3. RRDE profiles for Mn^{2+} collection experiments conducted at room temperature and 1000 rpm at spinel A ($LiMn_2O_4$) disc electrode cycled between 3.0 and 4.5 V at 100 mV s^{-1} and a ring electrode held at 1.0 V in 1 M $LiPF_6$ + EC/DMC (1:1) electrolyte, (I) cycles 1–10 (II) cycles 5–7.

ples are calculated from the CVs and exhibit an initial value of about 25 mAh g^{-1} on the first discharge. Only a fraction of the actual capacity is accessible at this high sweep rate. Samples B and C with cation-substituted spinel exhibit a moderate capacity loss of 0.2% per cycle over 200 cycles, i.e., half of the 0.4% per cycle experienced by sample A. Also, compared with the 58% loss in capacity for sample A, both B and C samples suffer about 37% capacity loss after 200 cycles. It has been demonstrated that the cation-substituted spinel cathodes have a good cycle-life in spite of some decreases in initial capacity.

The in situ monitoring of Mn dissolution from the spinel-based electrodes of samples A, B, and C was carried out during cycling voltammetry or galvanostatic charge and discharge by means of RRDE collection experiments. Figs. 3(I), 4(I) and 5(I) show both the disc voltage and ring current profiles for the first 10 cycles of the samples A, B and C, respectively, between 3.0 and 4.5 V with a sweep rate of 100 mV s^{-1} at room temperature. The ring electrode was held at 1.0 V with a rotation speed of 1000 rpm. In conjunction with the disc electrode, a regular shape of the ring current is observed after the first cycle for all samples, as shown in Figs. 3(I), 4(I) and 5(I). The cathodic peak current at the ring indicates that some Mn atoms are dissolved from the disc electrode into the electrolyte solution, to form soluble oxidized Mn^{+2} ion species that are reduced on the ring electrode.

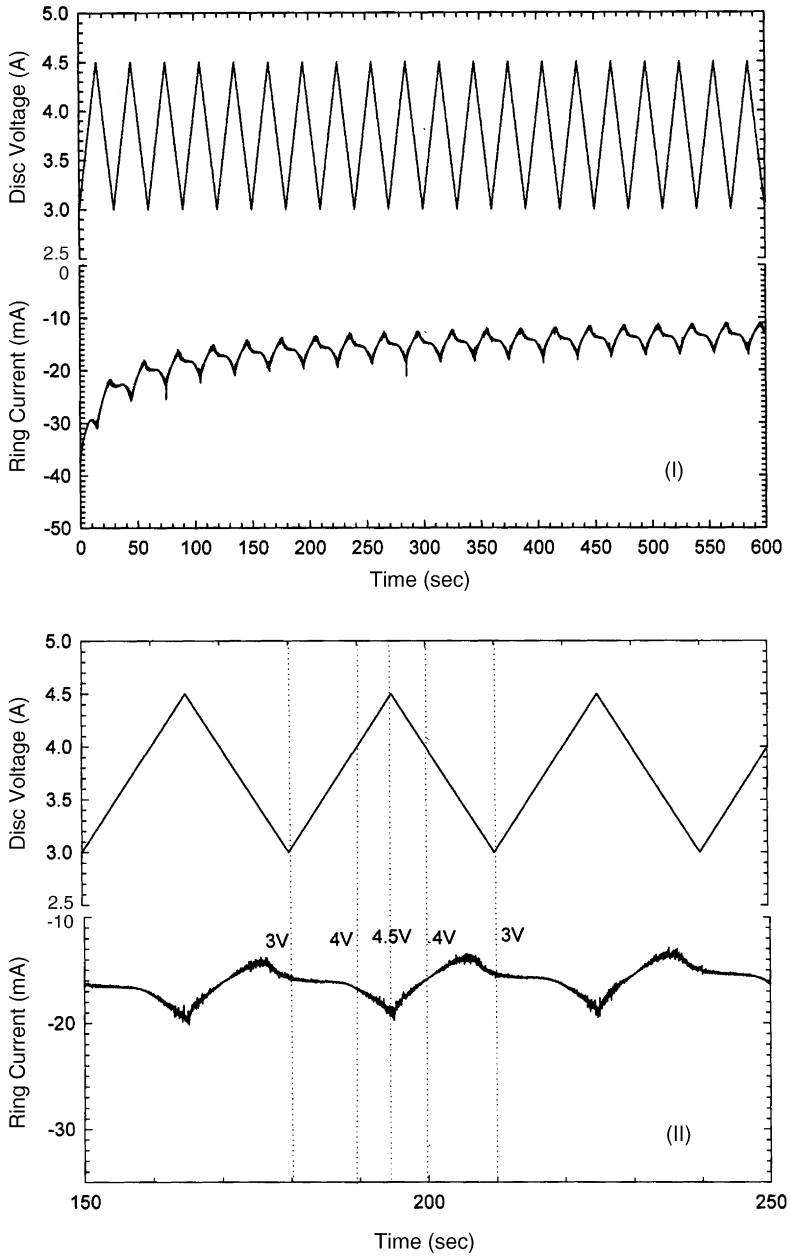

Fig. 4. RRDE profiles for Mn^{2+} collection experiments conducted at room temperature and 1000 rpm at spinel B ($Li_{1.07}Mn_{1.93}O_4$) disc electrode cycled between 3.0 and 4.5 V at 100 mV s^{-1} and a ring electrode held at 1.0 V in 1 M $LiPF_6$ + EC/DMC (1:1) electrolyte, (I) cycles 1–10 (II) cycles 5–7.

In all of the in situ studies, the first cycle exhibits a larger ring cathodic current due to the fresh Pt ring being more active for Mn^{+2} deposition. Expanded RRDE profiles for cycles 5, 6 and 7 are shown in Figs. 3(II), 4(II) and 5(II) for samples A, B, and C, respectively. Similar shaped ring cathodic currents are obtained for all samples, which exhibit the same Mn dissolution behaviour as the spinel-based cathode powders. The ring cathodic current increases from about 3.8 V (disc potential) and reaches a maximum when the disc potential is taken to 4.5 V during the charged process. On the cathodic sweep, the ring cathodic current becomes noticeable at a potential below 3.2 V (disc potential) and reaches a maximum when the disc potential drops to 3.0 V. The ring currents exhibit maxima corresponding to the end-of-charge (EOC) and end-of-discharge (EOD), with the largest peak at the EOC. These results indicate that dissolution of Mn from all the spinel electrodes is highest at the voltage end-points, with most of the Mn dissolution occurring at the EOC. This is in good agreement with most of the evidence reported thus far that points to solubility at the top of charge as the major reason for the capacity fading in Li/$LiMn_2O_4$-based cells.

Although similar maximum ring currents appear in the same region of the disc potential for all the spinel-based samples, there is a noticeable difference in the values of the ring cathodic currents. The ring cathodic currents in Fig. 3(II) are larger than those in Figs. 4(II) and 5(II), as expected for

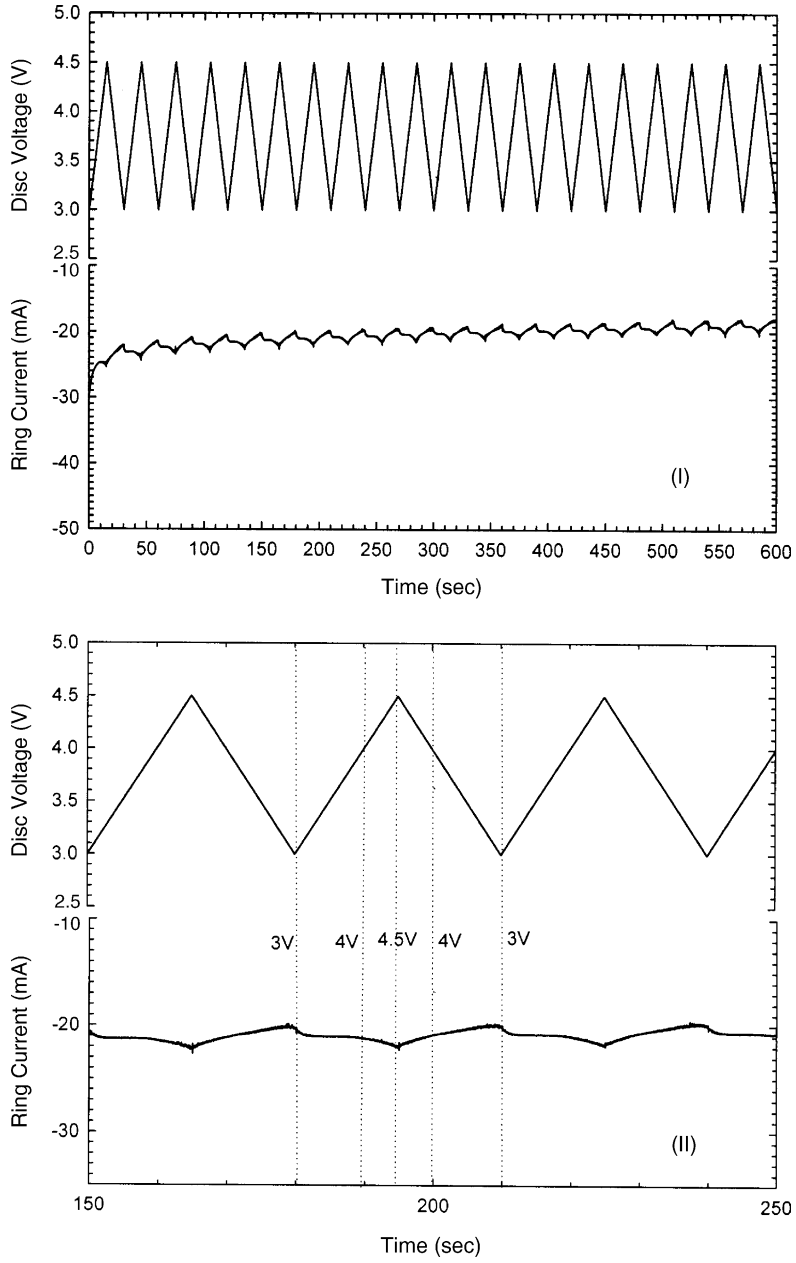

Fig. 5. RRDE profiles for Mn^{2+} collection experiments conducted at room temperature and 1000 rpm at spinel C ($Li_{1.06}Al_{0.2}Mn_{1.74}O_4$) disc electrode cycled between 3.0 and 4.5 V at 100 mV s^{-1} and a ring electrode held at 1.0 V in 1 M $LiPF_6$ + EC/DMC (1:1) electrolyte, (I) cycles 1–10 (II) cycles 5,6 and 7.

the cation-substituted samples (B and C). Obviously, this indicates that the dissolution of Mn rate is lower for the cation-substituted spinel materials. Moreover, the first few cycles experience a larger decay in the ring cathodic current (Fig. 3(I)), which suggests that the ring positioned at sample A is more active in Mn collection. This is in good agreement with most of the evidence reported thus far, which points to a decrease in solubility in cation-substituted spinel cathode powders [5,15,18,25–27]. Furthermore, Huang et al. [25] recently proposed that formation of a solid surface solution in cation-substituted spinel materials changed the surface properties of the spinel $LiMn_2O_4$ and suppressed the dissolution of the Mn^{+3} ions from the spinel into the electrolyte and the corresponding phase transitions.

In order to study the in situ monitoring of Mn dissolution during overcharge and overdischarge, the RRDE profile was examined between 2.0 and 5.0 V. Figs. 6(I), 7(I) and 8(I) show both the disc voltage and ring current profiles for the first 10 cycles of samples A, B and C, respectively, between 2.0 and 5.0 V with a sweep rate of 100 mV s^{-1} and room tem-

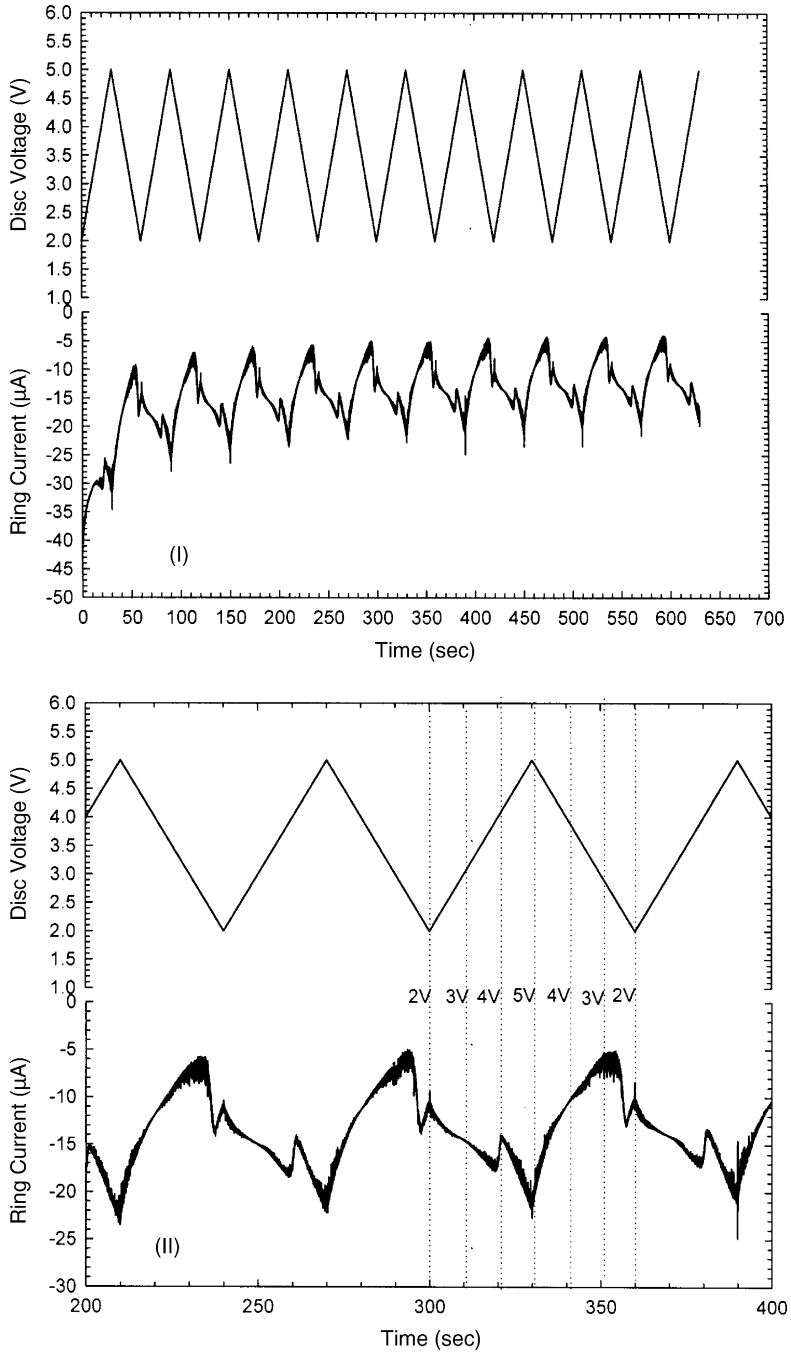

Fig. 6. RRDE profiles for Mn^{2+} collection experiments conducted at room temperature and 1000 rpm at spinel A ($LiMn_2O_4$) disc electrode cycled between 2.0 and 5.0 V at 100 mV s^{-1} and a ring electrode held at 1.0 V in 1 M $LiPF_6$ + EC/DMC (1:1) electrolyte, (I) cycles 1–10 (II) cycles 5,6 and 7.

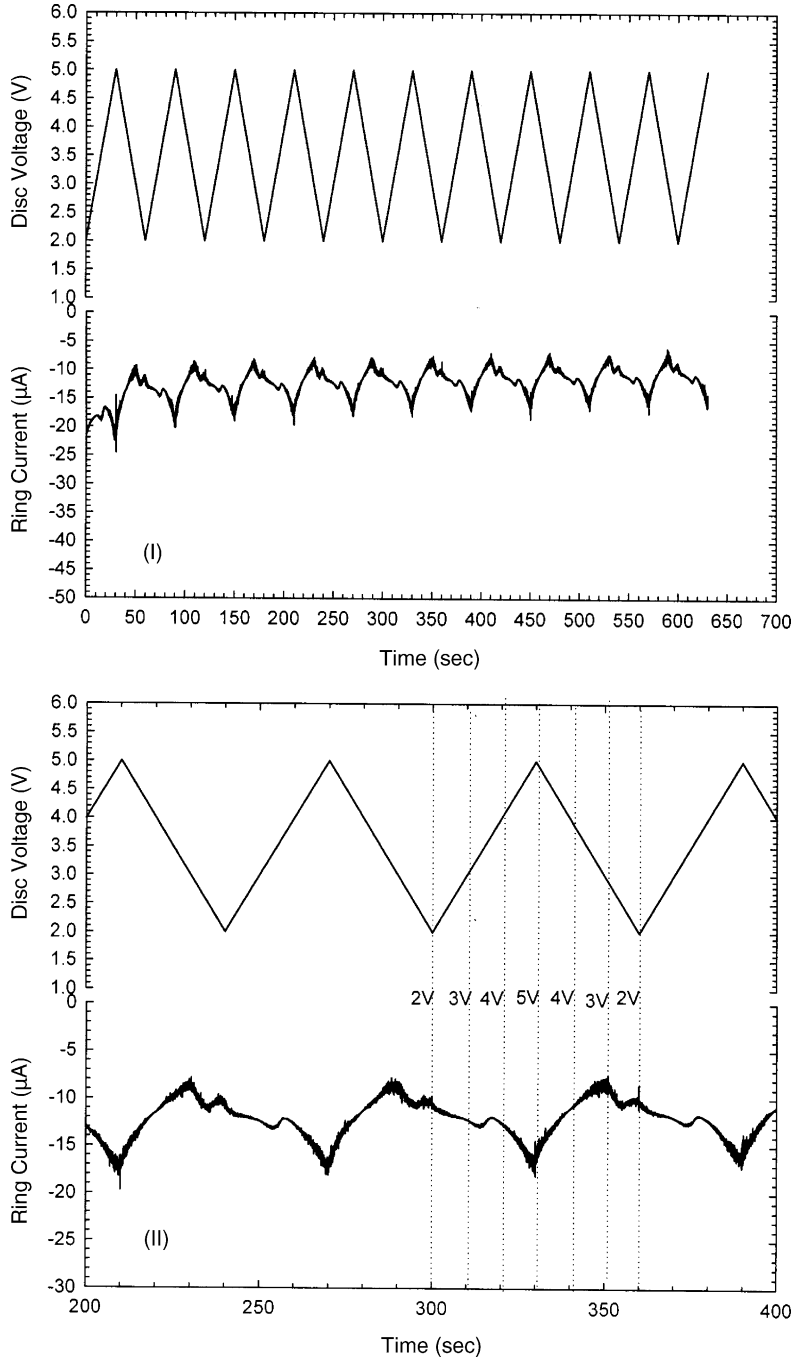

Fig. 7. RRDE profiles for Mn^{2+} collection experiments conducted at room temperature and 1000 rpm at spinel B ($Li_{1.07}Mn_{1.93}O_4$) disc electrode cycled between 2.0 and 5.0 V at 100 mV s^{-1} and a ring electrode held at 1.0 V in 1 M $LiPF_6$ + EC/DMC (1:1) electrolyte, (I) cycles 1–10 (II) cycles 5–7.

perature. Although a wide voltage window has been swept, similar results are obtained to those in the normal voltage sweep. In conjunction with the disc electrode, a regular shape of the ring current is observed after the first cycle for all samples, as shown in Figs. 6(I), 7(I) and 8(I). The corresponding expanded RRDE profiles for cycles 7, 8 and 9 are given in Figs. 6(II), 7(II) and 8(II). It is obvious that seven ring current maxima are observed for all samples over this voltage range. Those exhibiting Mn dissolution behaviour are similar for all samples during the cycling process. The first three peaks occur at disc potentials of 2.3, 3.9, and 5.0 V on the anodic sweep and the other four peaks at 4.5, 3.5, 2.9, and 2.3 V on the cathodic sweep. These observations suggest that the dissolution of Mn from all spinel-based electrodes takes place during the charging process, followed by the discharging process. From the experimental results, Mn dissolution from the spinel-based electrodes occurs at the end of the charging and discharging step. In particular, Mn dissolution is accelerated

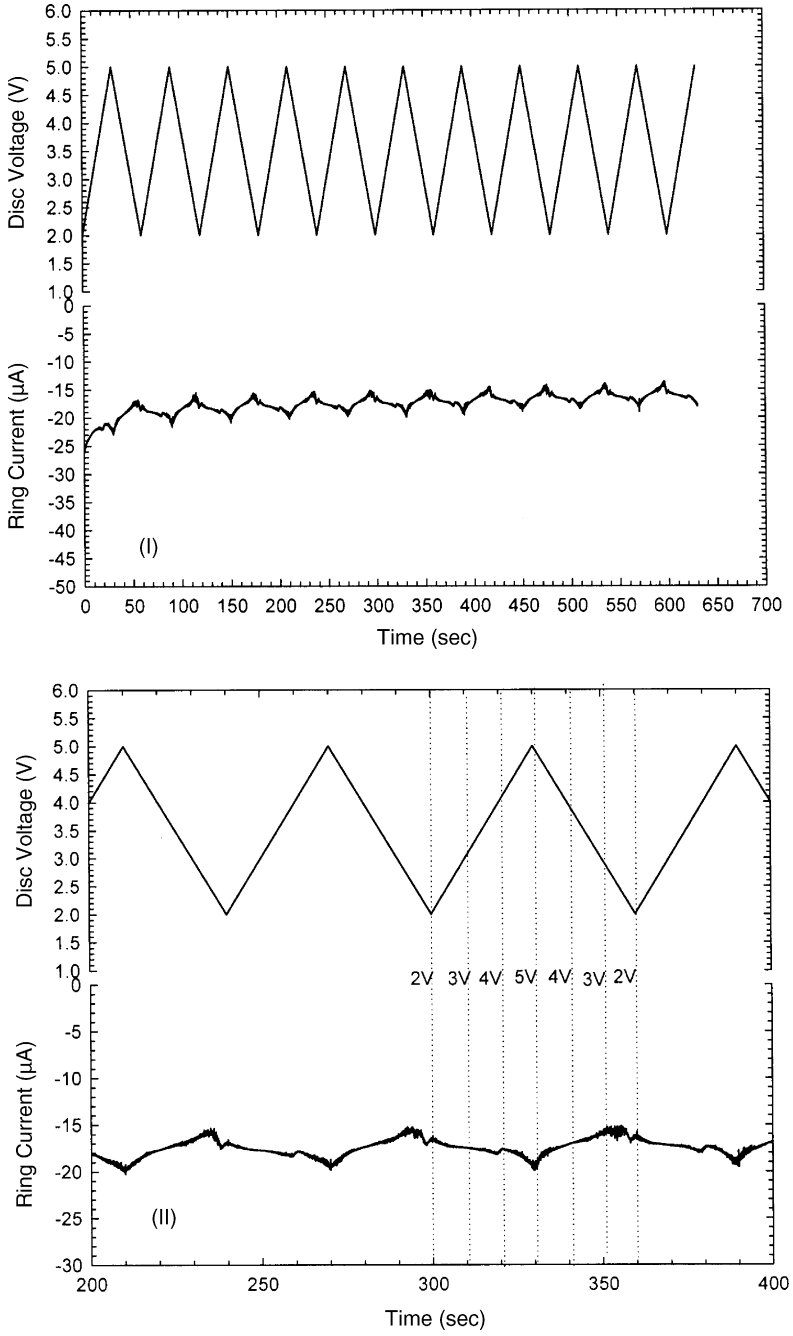

Fig. 8. RRDE profiles for Mn^{2+} collection experiments conducted at room temperature and 1000 rpm at spinel C ($Li_{1.06}Al_{0.2}Mn_{1.74}O_4$) disc electrode cycled between 2.0 and 5.0 V at 100 mV s^{-1} and a ring electrode held at 1.0 V in 1 M $LiPF_6$ + EC/DMC (1:1) electrolyte, (I) cycles 1–10 (II) cycles 5–7.

at the top of the charging stage and causes capacity fading. A similar dissolution tendency has been reported in many other papers [4,7–11].

4. Conclusion

The dissolution of Mn from a thin porous substituted spinel electrode is studied by rotating ring-disc collection experiments. Three types of spinel-based cathode powders, including the typical spinel $LiMn_2O_4$ and the cation-substituted spinel $Li_{1.07}Mn_{1.93}O_4$ and $Li_{1.06}Al_{0.2}Mn_{1.74}O_4$, have been investigated to measure Mn dissolution and capacity losses in lithium-ion cells. The capacities of all of the spinel-based samples are calculated from the CVs at a high sweep rate (10 mV s^{-1}) and exhibit an initial capacity of only about 25 mAh g^{-1} during the first discharge. The cation-substituted spinel experiences a moderate capacity loss of 0.2% per cycle over 200 cycles, i.e., were half of 0.4% per cycle for the typical spinel, $LiMn_2O_4$. It is clear that the cation-substituted

spinel cathodes have a good cycle-life despite some decrease in their initial capacity.

Manganese dissolution from all the spinel-based samples has been monitored in situ out under various conditions. Similar shaped ring cathodic currents are obtained for all samples, which exhibit the same Mn dissolution behaviour in the spinel-based cathode powders. The ring currents reach maxima at the EOC and EOD, with the largest peak at the former. The results suggest that the dissolution of Mn from all spinel-based samples occurs during charge–discharge cycling, especially in the charged state (at >4.0 V) and discharged state (at <3.1 V). The larger peak at the EOC demonstrates that Mn dissolution takes place mainly at the top of charge. Also, lower ring cathodic currents are observed in the cation-substituted spinel cathodes due to a decrease in the rate of Mn dissolution.

Acknowledgments

The authors are grateful to the National Science Council of the ROC for financial support to conduct this work under Contract No. NSC-91-2214-E-214-003. Thanks are also due to Forex Pro Enterprise Co. (Taiwan) for providing useful materials.

References

[1] Y. Nishi, J. Power Sources 100 (2001) 101–106.
[2] G. Pistoia, A. Antonini, R. Rosati, D. Zane, Electrochim. Acta 41 (1996) 2683.
[3] A. Antonini, C. Bellitto, M. Pasquali, G. Pistoia, J. Electrochem. Soc. 145 (1998) 2726.
[4] D.H. Jang, Y.J. Shin, S.M. Oh, J. Electrochem. Soc. 143 (1996) 2204.
[5] R.J. Gummow, A. de Kock, M.M. Tackeray, Solid State Ionics 69 (1994) 59.
[6] E. Wang, D. Ofer, W. Bowden, N. Iltchev, R. Moses, K. Brandt, J. Electrochem. Soc. 147 (2000) 4023.
[7] T. Aoshima, K. Okahara, C. Kiyohara, K. Shizuka, J. Power Sources 97–98 (2001) 377.
[8] Y. Xia, Y. Zhou, M. Yoshio, J. Electrochem. Soc. 144 (1997) 2593.
[9] A. Yamada, K. Miura, K. Hinokuma, M. Tanaka, J. Electrochem. Soc. 142 (1995) 2149.
[10] M.M. Thackeray, J. Electrochem. Soc. 142 (1995) 2558.
[11] G. Pistoia, G. Wang, Solid State Ionics 66 (1993) 135.
[12] Y. Gao, J.R. Dahn, J. Electrochem. Soc. 143 (1996) 100.
[13] J.M. Tarascon, F. Coowar, G. Amatucci, F.K. Shokoohi, D. Guyomard, J. Electrochem. Soc. 141 (1994) 1421.
[14] Y.J. Shin, A. Manthiram, Electrochem. Solid-State Lett. 5 (2002) A55–A58.
[15] H. Huang, C.A. Vincent, P.G. Bruce, J. Electrochem. Soc. 146 (1999) 3649–3654.
[16] L.-F. Wang, C.-C. Ou, K.A. Striebel, J.-S. Chen, J. Electrochem. Soc. 150 (2003) A905–A911.
[17] A.D. Pasquier, A. Blyr, P. Courjal, D. Larcher, G. Amatucci, B. Gerand, J.M. Tarascon, J. Electrochem. Soc. 146 (1999) 428.
[18] J.H. Lee, J.K. Hong, D.H. Jang, Y.K. Sun, S.M. Oh, J. Power Sources 89 (2000) 7.
[19] D.H. Jang, Y.J. Shin, S.M. Oh, J. Electrochem. Soc. 144 (1997) 3342.
[20] K. Dokko, S. Horikoshi, T. Itoh, M. Nishizawa, M. Mohamedi, I. Uchida, J. Power Sources 90 (2000) 109.
[21] J.-S. Chen, L.-F. Wang, J. Power Sources 70 (1998) 269–275.
[22] M. Saitoh, M. Sano, M. Fujita, M. Sakata, M. Takata, E. Nishibori, J. Electrochem. Soc. 151 (2004) A17–A22.
[23] M.M. Thackeray, S.H. Yang, A.J. Kahaian, K.D. Kepler, E. Skinner, J.T. Vaughey, S.A. Hackney, Electrochem. Solid-State Lett. 1 (1998) 7–9.
[24] Y.S. Lee, N.K. Kumada, M. Yoshio, J. Power Sources 96 (2001) 376–384.
[25] Y. Sun, Z. Wang, L. Chen, X. Huang, J. Electrochem. Soc. 150 (2003) A1294–A1298.
[26] K.A. Striebel, A. Rougier, C.R. Horne, R.F. Reade, E.J. Cairns, J. Electrochem. Soc. 146 (1999) 4339–4347.
[27] G.G. Amatucci, N. Pereira, T. Zheng, J.-M. Tarascon, J. Electrochem. Soc. 148 (2001) A171–A182.